




Steric Effects of Alcohols on the [Mn₄O₄] Cubane-Type Structures

Yan He , Zheng Zhou *  and Haixiang Han * 

Interdisciplinary Materials Research Center, School of Materials Science and Engineering, Tongji University, Shanghai 201804, China

* Correspondence: zhouzheng@tongji.edu.cn (Z.Z.); hxhan@tongji.edu.cn (H.H.)

Abstract: [M₄O₄] (M = 3d transition metal) represents an interesting class of compounds featuring cubane-type molecular structures, and particularly, [Mn₄O₄] cubanes or their derivatives attract much attention by virtue of their potential applications as single-molecule magnets (SMMs) or catalysts. However, the rational design of desired cubane-related structures is still a challenging subject due to the lack of readily available methods to effectively tune the construction patterns of the molecule assembly. In this work, we report the employment of different alcohols to prepare three cubane-related molecules, Mn₂(dhd)₄(ⁱPrOH)₂ (**1**), Mn₄(dhd)₄(OEt)₄(EtOH)₄ (**2**) and Mn₄(dhd)₆(OMe)₂(MeOH)₂ (**3**) (dhd = 5,5-dimethyl-2,4-hexanedione). Interestingly, the bulkiest ⁱPrOH leads to simple rhombic dimer molecule **1**. It can be deemed a rudimentary structure of tetranuclear [Mn₄O₄] cubane **2**, which can be realized by the use of less bulky EtOH. In addition, the least bulky MeOH promotes the assembly of the cubanes, eventually bringing about defective dicubane molecular cluster **3**. The accurate crystal structures of **1–3** were modeled by single-crystal X-ray diffraction, and their electronic structures were investigated through absorption spectroscopy coupled with theoretical calculations. Overall, this work demonstrates a systematic study on controlling cubane-type structures of Mn-based compounds by applying different solvents, which provides a new means to design functional molecules for specific applications.

Keywords: manganese complexes; cubane; single crystal; steric effect



Citation: He, Y.; Zhou, Z.; Han, H. Steric Effects of Alcohols on the [Mn₄O₄] Cubane-Type Structures. *Crystals* **2024**, *14*, 478. <https://doi.org/10.3390/cryst14050478>

Academic Editor: Sergey V. Krivovichev

Received: 29 April 2024

Revised: 10 May 2024

Accepted: 12 May 2024

Published: 19 May 2024



Copyright: © 2024 by the authors. Licensee MDPI, Basel, Switzerland. This article is an open access article distributed under the terms and conditions of the Creative Commons Attribution (CC BY) license (<https://creativecommons.org/licenses/by/4.0/>).

1. Introduction

Among the commonly studied 3D transition metals (e.g., Mn, Fe, Co and Ni), the chemistry of Mn is greatly attractive in three aspects: (i) Mn has the largest number of unpaired electrons in its 3D orbitals, affording novel electronic structures for phytochemical activities. (ii) Mn is able to demonstrate a wide range of oxidation states from 0 to up +7 in a substantial variety of readily accessible structures. (iii) The electron configurations in *e_g* orbitals for Mn^{III} make it unique to demonstrate Jahn–Teller distortion. Owing to these distinct natures, Mn-based materials have been broadly employed in applications. Over the past few decades, a number of manganese molecules and nano-sized clusters with nuclearities ranging from 2 to 84 have been successfully obtained [1–8]. Among them, molecular Mn-complexes, such as dinuclear, trinuclear and tetranuclear clusters, hold special positions among this family, and display promising properties in magnetism as single-molecule magnets (SMMs) [9–11] or catalysts [12,13]. Cubane-type molecules, such as the well-documented [Fe₄S₄] clusters, are biologically important because [Fe₄S₄] cubane units can act as important electron transistors in ferritins [14]. As for [Mn₄O₄] cubane-type molecules, they can also behave as good biocatalysts in the process of photosystem II [15,16].

In synthetic chemistry, targeting desired molecule structures through handleable means is of great importance in achieving true precision chemistry in the design of functional materials. For coordination complexes, ligands play significant roles in governing the overall structural characteristics of the molecules through steric hindrances or chelating/bridging patterns [17,18]. However, the solvents used in synthesis also act as bridging

ligands and are usually overlooked, which can also impose a significant influence on the resultant structure. Herein, we report three new Mn-based cubane-related molecular clusters and show how the alcohol solvents influence their final structures based on the steric effect.

2. Materials and Methods

2.1. Materials and Measurements

All of the manipulations were carried out in a dry, oxygen-free argon atmosphere by employing standard Schlenk and glove box techniques. Manganese chloride (MnCl_2 , 99.9%) was purchased from Sigma-Aldrich (St. Louis, MO, USA). 2,2-dimethyl-hexanedione (Hdhd, 99%), lithium methoxide (LiOMe, 99.9%), methanol (99.9%), ethanol (99.9%) and isopropanol (99.9%) were purchased from Adamas. UV-vis absorption (UV-vis) measurements were performed on an Agilent Cary 3500 spectrometer. All spectra were scanned at a rate of 1500 nm/min with a 1.0 nm interval and 2.0 nm spectral bandwidth.

2.2. Synthesis of $\text{Li}(\text{dhd})$

LiOMe (0.38 g, 10 mmol) was first dissolved in 15 mL of methanol, which was followed by the addition of Hdhd (1.5 mL 10 mmol). The solution was stirred for 24 h, which resulted in a yellow solution, indicating the formation of $\text{Li}(\text{dhd})$. The solvent was evaporated off and the resultant solid was dried in vacuo at 60 °C overnight. The yield was ca. 80.9% based on Li. The light-yellow powder of $\text{Li}(\text{dhd})$ had good solubility in most organic solvents such as methanol, ethanol, acetonitrile, acetone, dichloromethane (DCM) and hexane.

2.3. Synthesis of $\text{Mn}_2(\text{dhd})_4(^i\text{PrOH})_2$ (**1**)

A flask was loaded with a mixture of MnCl_2 (38.4 mg, 0.3 mmol) and $\text{Li}(\text{dhd})$ (104 mg, 0.6 mmol) under an argon atmosphere, and 5 mL of anhydrous, oxygen-free isopropanol ($^i\text{PrOH}$) was added to dissolve all the solids, which resulted in a transparent yellow solution after stirring for 6 h. The solvent was then evaporated off under vacuum at room temperature, which left a yellow residue in the flask. The final product was obtained by washing with anhydrous, oxygen-free DCM. The residue was further dried under vacuum at room temperature overnight. The yield was ca. 68.4% (based on Mn). Single crystals were grown directly from the reaction solution using a cooling method at 5 °C (see the Crystal Growth section in the Supplementary Materials for more information).

2.4. Synthesis of $\text{Mn}_4(\text{dhd})_4(\text{OEt})_4(\text{EtOH})_4$ (**2**)

This complex was synthesized in the same procedure as that used in **1** but using anhydrous, oxygen-free ethanol (EtOH) as the reaction solvent. The final product was obtained by washing with anhydrous, oxygen-free DCM. The residue was further dried under vacuum at room temperature overnight. The yield was ca. 65.3% (based on Mn). Single crystals were grown directly from the reaction solution using a cooling method at 5 °C (see the Crystal Growth section in the Supplementary Materials for more information).

2.5. Synthesis of $\text{Mn}_4(\text{dhd})_6(\text{OMe})_2(\text{MeOH})_2$ (**3**)

This complex was synthesized in the same procedure as that used in **1** but using anhydrous, oxygen-free methanol (MeOH) as the reaction solvent. The final product was obtained by washing with anhydrous, oxygen-free DCM. The residue was further dried under vacuum at room temperature overnight. The yield was ca. 71.3% (based on Mn). Single crystals were grown directly from the reaction solution using a cooling method at 5 °C (see the Crystal Growth section in the Supplementary Materials for more information).

2.6. X-ray Crystallographic Procedures

Data collection for **1** was performed on a Rigaku XtaLAB-Synergy-R X-ray diffractometer with a PHOTON 100 CMOS detector equipped with a Mo target. Data collection for **2** and **3** was performed on a Bruker D8 VENTURE X-ray diffractometer with a PHOTON 100 CMOS detector equipped with a Mo target. The Incoatec microfocus source

μ S X-ray tube ($\lambda = 0.71073 \text{ \AA}$) was used at $T = 150(2) \text{ K}$. Data reduction and integration were performed with the Bruker software package SAINT (version 8.38A) [19]. Data were corrected for absorption effects using the empirical methods implemented in SADABS (version 2016/2) [20]. The structure was solved using SHELXT [21] and refined via full-matrix least-squares procedures using the Bruker SHELXTL (version 2018/3) software package through the OLEX2 graphical interface [22]. All non-hydrogen atoms were refined anisotropically. The H-atoms were also included at calculated positions and refined using a riding model, with $U_{\text{iso}}(\text{H}) = 1.2 U_{\text{eq}}(\text{C})$. The anisotropic displacement parameters in the direction of the bonds were restrained to be equal with a standard uncertainty of 0.004 \AA . They were also restrained to have the same U_{ij} components, with a standard uncertainty of 0.01 \AA . Further crystal and data collection details are listed in Table 1. The crystal growth methods used in 1–3 can be found in the Supplementary Information (Supplementary Materials, Table S1).

Table 1. Crystal data and structure refinement parameters for 1–3.

Compound	1	2	3
CCDC	2351735	2351736	2351734
Moiety Formula	C ₃₈ H ₆₈ Mn ₂ O ₁₀ ·C ₃ H ₈ O	C ₄₈ H ₉₆ Mn ₄ O ₁₆	C ₅₂ H ₉₂ Mn ₄ O ₁₆
Formula weight	854.89	1149	1193.01
Temperature (K)	150	150	150
Wavelength (Å)	0.71073	0.71073	0.71073
Crystal system	Triclinic	Monoclinic	Monoclinic
Space group	P	P21/n	P21/n
<i>a</i> (Å)	10.621(2)	17.5839(13)	14.0445(8)
<i>b</i> (Å)	13.017(3)	17.189(10)	14.7969(8)
<i>c</i> (Å)	19.727(5)	21.0431(15)	15.6796(8)
α (°)	77.996(5)	90	90
β (°)	88.842(4)	107.029(2)	107.7926(2)
γ (°)	67.691(4)	90	90
<i>V</i> (Å ³)	2462.81(10)	6081.52(7)	3102.581(3)
<i>Z</i>	2	4	2
ρ_{calcd} (g·cm ^{−3})	1.153	1.255	1.277
μ (mm ^{−1})	0.562	0.869	0.854
<i>F</i> (000)	920	2448	1264
θ range for data collection (°)	1.058–25.098	2.422–21.124	2.75–25.53
Reflections collected	10,566	38,019	27,346
Independent reflections	7479 ($R_{\text{int}} = 0.0764$)	11115 ($R_{\text{int}} = 0.1252$)	8309 ($R_{\text{int}} = 0.0855$)
Transmission factors (min/max)	0.602/0.745	0.888/0.942	0.679/0.746
Data/restraints/params.	10,566/198/591	11,115/378/807	8309/3/342
$R1^a$, $wR2^b$ ($I > 2\sigma(I)$)	0.0640/0.1465	0.0708/0.1592	0.0525/0.1016
$R1^a$, $wR2^b$ (all data)	0.0455/0.1230	0.1235/0.2098	0.0855/0.1272
Goodness-of-fit ^c	1.077	1.043	1.030
Largest diff. peak and hole ($\text{e} \cdot \text{\AA}^{-3}$)	0.447 and −0.442	0.683 and −0.382	0.531 and −0.448

^a $R1 = \sum ||F_o| - |F_c|| / \sum |F_o|$. ^b $wR2 = [\sum [w(F_o^2 - F_c^2)^2] / \sum [w(F_o^2)^2]]^{1/2}$. ^c Goodness-of-fit = $[\sum [w(F_o^2 - F_c^2)^2] / (N_{\text{o-s}} - N_{\text{params}})]^{1/2}$, based on all data.

3. Results and Discussion

3.1. Synthesis

Alkoxides with a general formula of ROH (R = alkyl group) can not only act as the σ -donating ligands to coordinate metal centers, but also bridge metal atoms to integrate the entire cubic entity. The bridging pattern for the alkoxide can play critical roles in modulating entire molecular structures. For example, Driess and co-workers have reported that the use of ROH alcohols, with the R groups being ^{*t*}Propyl, ^{*t*}Butyl and ^{*C*}Hexyl, results in a single [Mg₄O₄] cubane, while a [Mg₇O₈] dicubane-type structure can be obtained when

the R groups are the less bulky Ethyl, ⁿPropyl or ⁿButyl groups [23]. The subtle change of the alkyl group R on alkoxides could bring about significant variations in stereochemistry or coordination strength to alkoxides, which in turn tunes their bridging behavior to the metal centers and eventually results in different molecule structures [23,24]. In our works, we used dhd (dhd = 5,5-dimethyl-2,4-hexanedione) and a series of alcohols (methanol (CH₃OH), ethanol (CH₃CH₂OH) and isopropanol (CH₃)₂HCOH)) to prepare three different molecules. It was revealed that a relatively bulky R group could hinder the production of the three-dimensional geometry, giving rise to a two-dimensional rhombic subunit of [Mn₂O₂] for a typical full [Mn₄O₄] cubane, while small R groups seemed to promote the formation of intact cubic or even defective dicubane [25] structures. Briefly, the use of isopropanol leads to a dinuclear rhombic complex, Mn₂(dhd)₄(ⁱPrOH)₂ (**1**), whereas ethanol and methanol result in a cubic Mn₄(dhd)₄(OEt)₄(EtOH)₄ (**2**) and a “defective dicubic” Mn₄(dhd)₆(OMe)₂(MeOH)₂ (**3**) molecule, respectively (Figure 1). Of note, compound **3** can be considered a preliminary extension of the close cubic topology, which implies a possibility of continuous growth of cubanes under appropriate conditions.

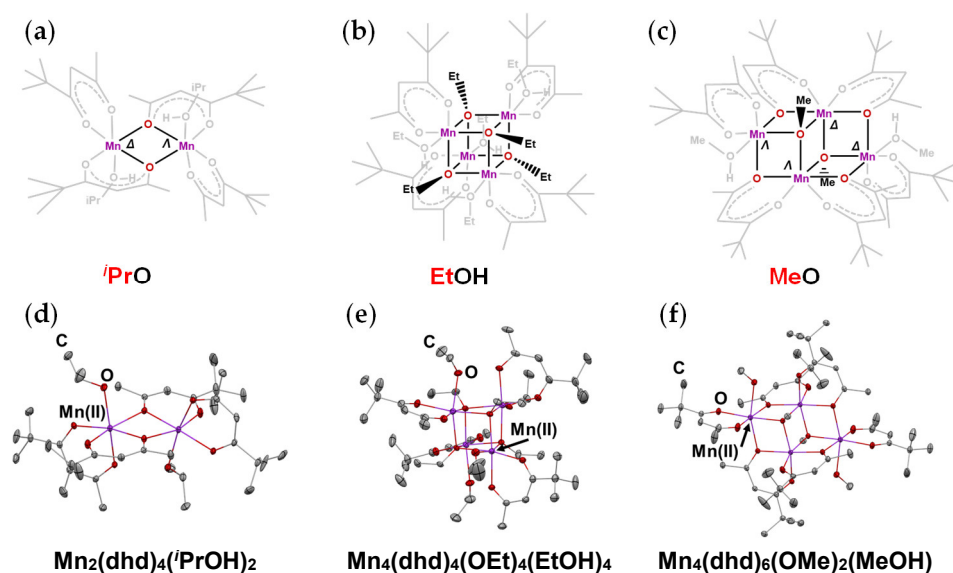
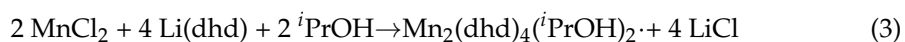
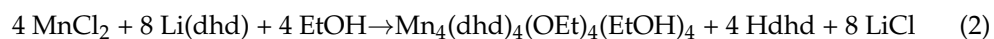
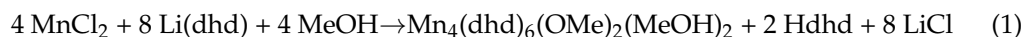


Figure 1. Schematic and solid-state structures of molecules **1**, **2** and **3**. (a–c): Schematic structures of **1–3**. Colored elements and black bonds highlight the cores of the three structures and their alkoxide ligands. (d–f): Single-crystal structures of **1–3** drawn with thermal ellipsoids at the 30% probability level. H atoms were omitted for clarity. Mn^{II}, purple; O, red; C, grey.

Compounds **1–3** can be effectively prepared in a high yield through solution reactions by employing readily available MnCl₂ and homoleptic complex Li(dhd) in the respective alcohols (Equations (1)–(3)):

The alcohols are used as both solvents and starting reactants. In a general preparation process, a mixture of MnCl₂ and Li(dhd) solids was first loaded in a flask, which was followed by the addition of the alcohol. The solids were completely dissolved to yield a transparent, yellow solution, after which the solvent was evaporated off at room temperature and the solid residues were redissolved in DCM. At this step, the byproduct LiCl could be effectively eliminated by filtration as it was not soluble in DCM. The final solid products were obtained after the evaporation of DCM at ambient temperature and dried under vacuum overnight. (see Supplementary Materials for more information). Molecules **1–3** appear as yellow in color and demonstrate good solubility in commonly used solvents, such as alcohols, acetone, DCM or hexane. They are relatively stable in open air in a solid

state, but become extremely sensitive in solution, immediately turning dark upon exposure to the air, suggesting the oxidation of divalent Mn to trivalent Mn.



3.2. Single Crystal Structures of 1, 2 and 3

Single-crystal X-ray diffraction analysis revealed that compound **1** crystallizes into a centrosymmetric space group of $P\bar{1}$. Each Mn center displays an octahedron coordination environment with two chelating dhd diketonates and a neutral σ -donating ${}^i\text{PrOH}$ molecule. The Mn cations are also bridged by the neighboring dhd ligand chelating on another Mn cation through the oxygen atom. Such a coordination pattern results in chirality for each Mn center, displaying either a Δ - or Λ -chiral configuration (Figure 1a). It is interesting to note that dhd represents an unsymmetric β -diketonate ligand, where the substituent groups on the two sides feature different bulkiness (Supplementary Materials, Figures S4 and S5). The relatively bulkier group, such as ${}^t\text{butyl}$ or $\text{O}{}^t\text{butyl}$, effectively prevents the proximal O atom from bridging to other metals, confining it to a pure chelating mode, while oxygen near the less bulky side (e.g., CH_3 or CF_3) is able to participate in both chelating and bridging interactions [26,27]. The dhd ligands in compound **1** obey the same rule that states that only the oxygen atom near the methyl group demonstrates bridging behavior. Dinuclear molecule **1** obtained from the relatively bulky isopropanol has a rhombic $[\text{Mn}_2\text{O}_2]$ structure, and can be deemed the subunit of the cubic molecule assembly [28]. Performing the reaction in ethanol resulted in a typical cubic molecular structure of **2** (Figure 1b,e), which crystallized into a monoclinic space group, $P2_1/n$, and showed a cubic geometry with the four Mn atoms being linked by four methoxides through $\mu^3\text{-O}$ at the alternating vertices of the cube. Each Mn metal was also chelated by a dhd ligand and donated by a neutral methanol molecule, displaying an octahedron coordination environment. Such a $[\text{M}_4\text{O}_4]$ cubic structural character has also been found in other metals, such as $[\text{Co}^{\text{III}}_4\text{O}_4(\text{OAc})_4\text{py}_4]$ [29], $[\text{Zn}_4{}^t\text{BuO}_4\text{Me}_4]$ [30], $[\text{Fe}^{\text{II}}_4(\text{hmp})_4(\text{MeOH})_4\text{Cl}_4]$ [31], etc. Continuously reducing the size of the R group to the methyl substituent, that is, using methanol as the least bulky alcohol, eventually yields a “defective dicubane” tetranuclear molecule due to the sharing of a common square face (Figure 1c,f). The two cubic units each miss one Mn vertice, demonstrating an overall “defective dicubane” geometry. Akin to compound **2**, the entire dicubic assembly also features a $[-\text{Mn}-\text{O}-]$ framework wherein the bridging oxygens from methoxides are in a μ^3 -bridging mode. In molecule **3**, all four Mn metals show an octahedron coordination environment. The two Mn vertices located on the shared square plane are chelated by two dhd ligands and bridged by two methoxides, while the other two Mn vertices are bridged by a dhd ligand and two methoxides, and chelated by a dhd ligand. At the same time, a neutral methanol molecule is also involved in the coordination interaction, providing an σ -donating O molecule to the metal center. Such a “defective dicubane” structure signifies the simplest assembly mode of the cubic units as they started to display the manner of fusion by sharing one face.

Detailed bond distance inspection (Table 2) clearly reveals the divalent nature of the Mn atoms in molecules **1–3**. The absence of the Jahn–Teller effect for the Mn centers and their relatively longer averaged Mn–O bond distances can reliably rule out the presence of trivalent Mn cations. In particular, $\text{Mn}^{\text{II}}\text{-O}_{\text{dhd}}$ (chelating) bond distances in three compounds range from 2.133 Å to 2.151 Å, while the $\text{Mn}^{\text{III}}\text{-O}_{\text{thd}}$ (chelating) bond distances in related compounds are obviously shorter, usually falling into the range of 1.901 Å to 2.036 Å. In compounds **1** and **3**, the dhd ligands also display a bridging interaction with the neighboring Mn ligands through the oxygen ligands, exhibiting the averaged $\text{Mn}^{\text{II}}\text{-O}_{\text{dhd}}$ (bridging) bond distances of 2.208 Å and 2.249 Å. However, the Mn–O_{OR} and Mn–O_{ROH} bond lengths in the three compounds vary considerably depending on the different alcohols

incorporated in the molecular structures. For example, the averaged Mn–O_{ROH} bond distances from the donating neutral alcohols are 2.201 Å, 2.257 Å and 2.278 Å for compounds **1**, **2** and **3**, respectively, displaying an increasing trend when the alcohols become less bulky. It is interesting to address here that the averaged Mn–O_{OR} bond distance in **3** is significantly shorter than that in compound **2** (2.191 Å vs. 2.147 Å), though the oxygens from RO[−] all present a μ^3 -bridging mode. Such a bridging pattern is important for the construction of three-dimensional cubane characteristics. It might imply that among different alcohols, methanol is superior in forming stable Mn–O_{OR} bonds, thereby facilitating the structure growth from cubane to defective dicubane.

Table 2. Comparison of the averaged Mn–O distances of **1**, **2**, **3** and related compounds.

Mn–O Bond Length	1	2	3	LiMn ₂ (thd) ₅ [32]	Mn(thd) ₃ [33]
Mn–O _{dhd} (chelating)	2.149	2.150	2.133	/	/
Mn–O _{dhd} (bridging)	2.209	/	2.249	/	/
Mn–O _{OR}	/	2.191	2.147	/	/
Mn–O _{ROH}	2.202	2.254	2.278	/	/
Mn–O _{total}	2.168	2.188	2.168	/	/
Mn ^{II} –O _{thd}	/	/	/	2.176	/
Mn ^{III} –O _{thd}	/	/	/	/	1.988

3.3. Electronic Structures

Absorption spectra were measured to understand the optical properties of **1–3** (Figure 2). DFT calculations were carried out to further understand their electronic structures using the PBE hybrid functional [34] in conjunction with the def2-TZVP basis set [35]. In all three structures, as shown in the partial density of states (Figure 3), the highest occupied orbitals are dominated by *d* shells from Mn atoms, while the lowest unoccupied orbitals are mainly from a combination of *p* of the O atom and *d* of the Mn atom, which is a result of partially filled *d* orbitals in Mn^{II}. By comparing the orbital composition of **1–3**, the higher LUMOs are concentrated on ligands (Tables S5–S7). It was revealed that the major electron transition of these complexes arises from ligand-to-metal charge transfer, which is commonly seen in the reported Mn^{II} complexes, while the *d–d* transitions around 450 nm can barely be seen. For instance, the major transition in **1** is from HOMO to LUMO + 1 with a large energy gap of 3.30 eV, which correlates well with the absorption peak observed in the UV-vis experiment (370 nm). In contrast, major electron transitions of HOMO → LUMO + 2 indicate that LMCT are found in **2** and **3**.

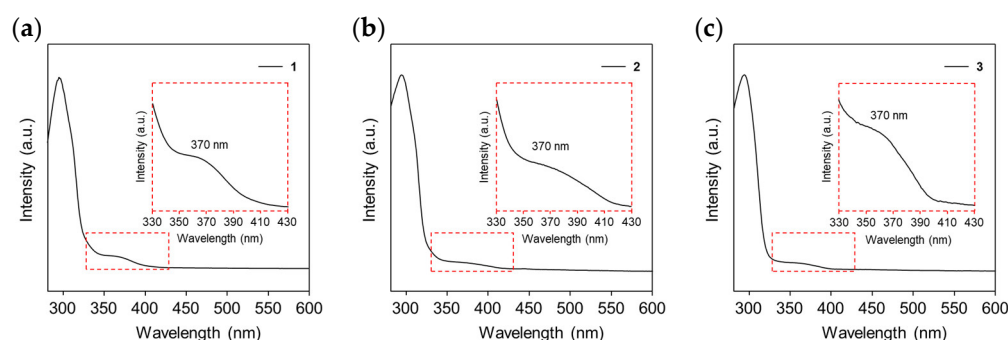


Figure 2. UV-vis spectra of (a) **1**/*i*PrOH solution, (b) **2**/EtOH solution and (c) **3**/MeOH solution.

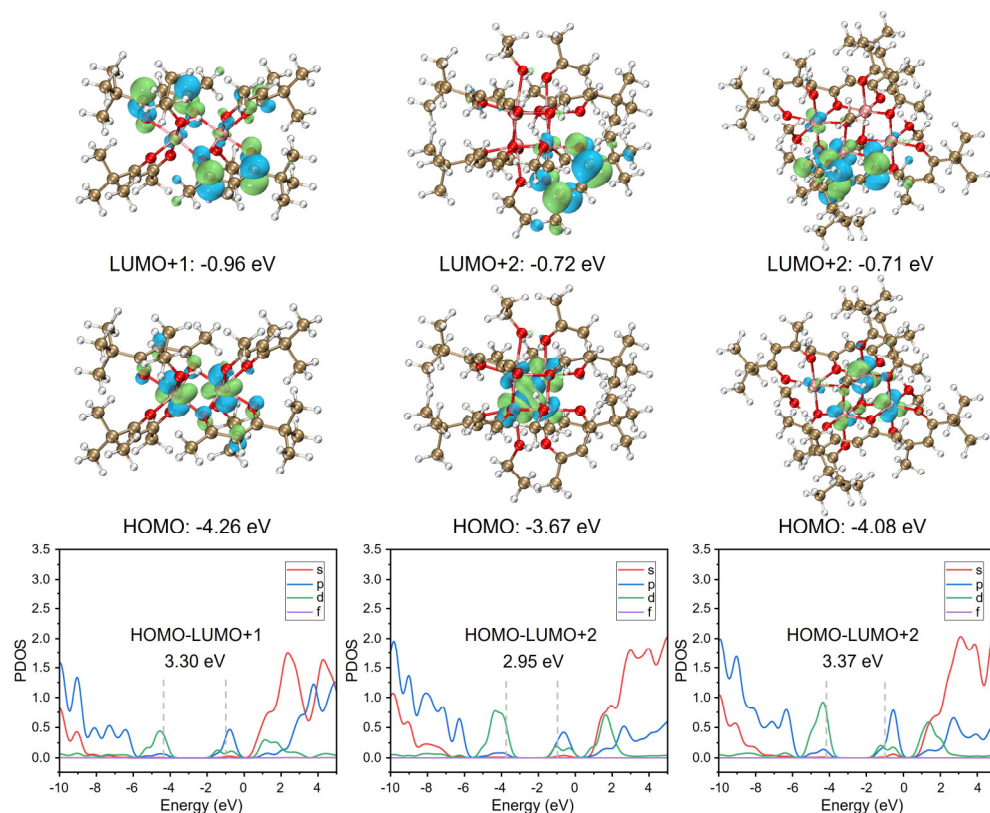


Figure 3. Frontier molecular orbitals (LUMO and HOMO) and partial density of states in 1–3 with energy gaps.

Although those molecule structures are hardly considered “completely new”, this is the first systematic investigation that clearly reveals the influence of the ligands on the cubane-type Mn–O molecules. The acquisition of three compounds, achieved by employing different alcohols, may hint at two conclusions: (i) alkoxides can effectively participate in the construction of cubic or cube-assembled structures through the bridging pattern, and (ii) the less bulky alcohol may foster the assembling of cubic units. DFT calculations were carried out to gain insights into the influence of alcohol ligands on the structures. The rhombic, cubic and defective dicubic structures were each constructed with three types of alkoxide ligands (MeOH/MeO, EtOH/EtO, and *i*PrOH/*i*PrO), and their relative energies were calculated by unifying these structures with the same H atoms (Supplementary Materials, Figure S6 and Table S8). It was revealed that energetically, the simplest rhombic structure is prone to incorporating the bulkiest *i*PrO[−] ligands, while the least bulky CH₃O[−] is more favorable for fostering the formation of the cubic and the defective dicubic structures, despite the fact that we did not experimentally obtain the analog of molecule 2 with methanol. It should be noted that upon the growth of the clusters, the steric effect of organic ligands becomes more profound, and methoxide is more appropriate in the construction of high-nuclearity clusters in this regard.

4. Conclusions

In conclusion, three cubane-type molecular clusters were successfully prepared through a one-pot synthetic approach. It is interesting to observe that steric effects that stem from the ligands are of great importance in governing the overall structures of the resultant molecules. In this work, we show that the alcohol with the bulkiest alkyl group results in the simplest rhombic dimer, while the least bulky alcohol fosters the construction of cubane-type units into a defective dicubane molecular assembly. This work provides new ways to manipulate molecule structures by employing different organic ligands with different steric hindrances.

Supplementary Materials: The following supporting information can be downloaded at <https://www.mdpi.com/article/10.3390/cryst14050478/s1>: Table S1: Crystal data and structure refinement parameters for 1–3; Figure S1: Solid-state structure of 1 drawn with the thermal ellipsoids at the 40% probability level. Hydrogen atoms are represented by spheres of arbitrary radius. Only metal and oxygen atoms are labeled. Mn^{II}, purple; O, red; C, grey; H, white; Table S2: Selected bond distances in structure 1; Figure S2: Solid-state structure of 2 drawn with the thermal ellipsoids at the 40% probability level. Hydrogen atoms are represented by spheres of arbitrary radius. Only metal and oxygen atoms are labeled. Mn^{II}, purple; O, red; C, grey; H, white; Table S3: Selected bond distances in structure 2; Figure S3: Solid-state structure of 3 drawn with thermal ellipsoids at the 40% probability level. Hydrogen atoms are represented by spheres of an arbitrary radius. Only metal and oxygen atoms are labeled. Mn^{II}, purple; O, red; C, grey; H, white; Table S4: Selected bond distances in structure 3; Figure S4: Symmetric and unsymmetric diketones and their molecular structures; Figure S5: Steric hindrance caused by bulky side of diketones and its impacts on binding patterns; Table S5: Orbital composition analysis in 1; Table S6: Orbital composition analysis in 2; Table S7: Orbital composition analysis in 3; Table S8: Energy comparison of 1–3 with different alcohol/alkoxide ligands; Figure S6: Theoretical calculations for relative energies of rhombic, cubic and defective dicubic structures with different alcohol/alkoxide ligands; Table S9: Cartesian coordinates of the H-substituted 1-Me; Table S10: Cartesian coordinates of the H-substituted 1-Et; Table S11: Cartesian coordinates of the H-substituted 1-ⁱPr; Table S12: Cartesian coordinates of the H-substituted 2-Me; Table S13: Cartesian coordinates of the H-substituted 2-Et; Table S14: Cartesian coordinates of the H-substituted 2-ⁱPr; Table S15: Cartesian coordinates of the H-substituted 3-Me; Table S16: Cartesian coordinates of the H-substituted 3-Et; Table S17: Cartesian coordinates of the H-substituted 3-ⁱPr. References [34–37] are cited in the supplementary materials.

Author Contributions: Y.H. conducted synthesis, crystal growth, and absorption spectroscopy; Z.Z. performed theoretical calculations and analyzed electronic structures. H.H. conceived this project, supervised and guided the design, analysis, interpretation and wrote the manuscript. All authors contributed to the interpretation of the results and preparation of the manuscript. All authors have read and agreed to the published version of the manuscript.

Funding: This work is supported by the Fundamental Research Funds for the Central Universities (22120240204 and 22120240039), the National Natural Science Foundation of China (22301219, Z.Z.; 22101205, H.H.).

Data Availability Statement: The raw data supporting the conclusions of this article will be made available by the authors on request.

Conflicts of Interest: The authors declare no conflicts of interest.

References

1. Wu, J.-Z.; Sellitto, E.; Yap, G.P.A.; Sheats, J.; Dismukes, G.C. Trapping an Elusive Intermediate in Manganese–Oxo Cubane Chemistry. *Inorg. Chem.* **2004**, *43*, 5795–5797. [[CrossRef](#)]
2. Sessoli, R.; Tsai, H.L.; Schake, A.R.; Wang, S.; Vincent, J.B.; Folting, K.; Gatteschi, D.; Christou, G.; Hendrickson, D.N. High-Spin Molecules: [Mn₁₂O₁₂(O₂CR)₁₆(H₂O)₄]. *J. Am. Chem. Soc.* **1993**, *115*, 1804–1816. [[CrossRef](#)]
3. Lampropoulos, C.; Koo, C.; Hill, S.O.; Abboud, K.; Christou, G. Synthesis, Magnetism, and High-Frequency EPR Spectroscopy of a Family of Mixed-Valent Cuboctahedral Mn₁₃ Complexes with 1,8-Naphthalenedicarboxylate Ligands. *Inorg. Chem.* **2008**, *47*, 11180–11190. [[CrossRef](#)]
4. Brechin, E.K.; Clegg, W.; Murrie, M.; Parsons, S.; Teat, S.J.; Winpenny, R.E.P. Nanoscale Cages of Manganese and Nickel with “Rock Salt” Cores. *J. Am. Chem. Soc.* **1998**, *120*, 7365–7366. [[CrossRef](#)]
5. Soler, M.; Wernsdorfer, W.; Folting, K.; Pink, M.; Christou, G. Single-Molecule Magnets: A Large Mn₃₀ Molecular Nanomagnet Exhibiting Quantum Tunneling of Magnetization. *J. Am. Chem. Soc.* **2004**, *126*, 2156–2165. [[CrossRef](#)]
6. Stamatatos, T.C.; Abboud, K.A.; Wernsdorfer, W.; Christou, G. “Spin Tweaking” of a High-Spin Molecule: An Mn₂₅ Single-Molecule Magnet with an S = 61/2 Ground State. *Angew. Chem. Int. Ed.* **2007**, *46*, 884–888. [[CrossRef](#)]
7. Manoli, M.; Alexandrou, S.; Pham, L.; Lorusso, G.; Wernsdorfer, W.; Evangelisti, M.; Christou, G.; Tasiopoulos, A.J. Magnetic “Molecular Oligomers” Based on Decametallate Supertetrahedra: A Giant Mn₄₉ Cuboctahedron and its Mn₂₅Na₄ Fragment. *Angew. Chem. Int. Ed.* **2016**, *55*, 679–684. [[CrossRef](#)] [[PubMed](#)]
8. Tasiopoulos, A.J.; Vinlava, A.; Wernsdorfer, W.; Abboud, K.A.; Christou, G. Giant Single-Molecule Magnets: A {Mn₈₄} Torus and Its Supramolecular Nanotubes. *Angew. Chem. Int. Ed.* **2004**, *43*, 2117–2121. [[CrossRef](#)] [[PubMed](#)]
9. Miyasaka, H.; Clérac, R.; Wernsdorfer, W.; Lecren, L.; Bonhomme, C.; Sugiura, K.-i.; Yamashita, M. A Dimeric Manganese(III) Tetratetrate Schiff Base Complex as a Single-Molecule Magnet. *Angew. Chem. Int. Ed.* **2004**, *43*, 2801–2805. [[CrossRef](#)] [[PubMed](#)]

10. Lecren, L.; Roubeau, O.; Coulon, C.; Li, Y.-G.; Le Goff, X.F.; Wernsdorfer, W.; Miyasaka, H.; Clérac, R. Slow Relaxation in a One-Dimensional Rational Assembly of Antiferromagnetically Coupled [Mn₄] Single-Molecule Magnets. *J. Am. Chem. Soc.* **2005**, *127*, 17353–17363. [[CrossRef](#)]
11. Zhou, C.-L.; Wang, Z.-M.; Wang, B.-W.; Gao, S. A Oximate-Bridged Linear Trinuclear [Mn^{IV}Mn^{III}Mn^{IV}] Single-Molecule Magnet. *Dalton Trans.* **2012**, *41*, 13620–13625. [[CrossRef](#)] [[PubMed](#)]
12. Dismukes, G.C.; Brimblecombe, R.; Felton, G.A.N.; Pryadun, R.S.; Sheats, J.E.; Spiccia, L.; Swiegers, G.F. Development of Bioinspired Mn₄O₄–Cubane Water Oxidation Catalysts: Lessons from Photosynthesis. *Acc. Chem. Res.* **2009**, *42*, 1935–1943. [[CrossRef](#)] [[PubMed](#)]
13. Hocking, R.K.; Brimblecombe, R.; Chang, L.-Y.; Singh, A.; Cheah, M.H.; Glover, C.; Casey, W.H.; Spiccia, L. Water-Oxidation Catalysis by Manganese in a Geochemical-Like Cycle. *Nat. Chem.* **2011**, *3*, 461–466. [[CrossRef](#)] [[PubMed](#)]
14. Holm, R.H.; Lo, W. Structural Conversions of Synthetic and Protein-Bound Iron–Sulfur Clusters. *Chem. Rev.* **2016**, *116*, 13685–13713. [[CrossRef](#)] [[PubMed](#)]
15. Mukhopadhyay, S.; Mandal, S.K.; Bhaduri, S.; Armstrong, W.H. Manganese Clusters with Relevance to Photosystem II. *Chem. Rev.* **2004**, *104*, 3981–4026. [[CrossRef](#)] [[PubMed](#)]
16. Chernev, P.; Fischer, S.; Hoffmann, J.; Oliver, N.; Assunção, R.; Yu, B.; Burnap, R.L.; Zaharieva, I.; Nürnberg, D.J.; Haumann, M.; et al. Light-Driven Formation of Manganese Oxide by Today’s Photosystem II Supports Evolutionarily Ancient Manganese-Oxidizing Photosynthesis. *Nat. Commun.* **2020**, *11*, 6110. [[CrossRef](#)] [[PubMed](#)]
17. Mayilmurugan, R.; Suresh, E.; Palaniandavar, M. A New Tripodal Iron(III) Monophenolate Complex: Effects of Ligand Basicity, Steric Hindrance, and Solvent on Regioselective Extradial Cleavage. *Inorg. Chem.* **2007**, *46*, 6038–6049. [[CrossRef](#)] [[PubMed](#)]
18. Ren, Y.-P.; Kong, X.-J.; Hu, X.-Y.; Sun, M.; Long, L.-S.; Huang, R.-B.; Zheng, L.-S. Influence of Steric Hindrance of Organic Ligand on the Structure of Keggin-Based Coordination Polymer. *Inorg. Chem.* **2006**, *45*, 4016–4023. [[CrossRef](#)] [[PubMed](#)]
19. SAINT. Part of Bruker APEX3 Software Package, (Version 2016.9-0); Bruker AXS: Billerica, MA, USA, 2016.
20. SADABS. Part of Bruker APEX3 Software Package, (Version 2016.9-0); Bruker AXS: Billerica, MA, USA, 2016.
21. Sheldrick, G.M. SHELXT–Integrated Space-Group and Crystal-Structure Determination. *Acta Crystallogr. Sect. A* **2015**, *71*, 3–8. [[CrossRef](#)]
22. Sheldrick, G. Crystal Structure Refinement with SHELXL. *Acta Crystallogr. Sect. C* **2015**, *71*, 3–8. [[CrossRef](#)]
23. Heitz, S.; Aksu, Y.; Merschjann, C.; Driess, M. Methylmagnesium Alkoxide Clusters with Mg₄O₄ Cubane- and Mg₇O₈ Biscubane-Like Cores: Organometallic Precursors for Low-Temperature Formation of MgO Nanoparticles with Variable Surface Defects. *Chem. Mater.* **2010**, *22*, 1376–1385. [[CrossRef](#)]
24. Kitos, A.A.; Papatriantafyllopoulou, C.; Tasiopoulos, A.J.; Perlepes, S.P.; Escuer, A.; Nastopoulos, V. Binding of Ligands Containing Carbonyl and Phenol Groups to Iron(III): New Fe₆, Fe₁₀ and Fe₁₂ Coordination Clusters. *Dalton Trans.* **2017**, *46*, 3240–3251. [[CrossRef](#)] [[PubMed](#)]
25. Serna, Z.; De la Pinta, N.; Urriaga, M.K.; Lezama, L.; Madariaga, G.; Clemente-Juan, J.M.; Coronado, E.; Cortés, R. Defective Dicubane-like Tetranuclear Nickel(II) Cyanate and Azide Nanoscale Magnets. *Inorg. Chem.* **2010**, *49*, 11541–11549. [[CrossRef](#)] [[PubMed](#)]
26. Han, H.; Wei, Z.; Barry, M.C.; Filatov, A.S.; Dikarev, E.V. Heterometallic Molecular Precursors for a Lithium–Iron Oxide Material: Synthesis, Solid State Structure, Solution and Gas-Phase Behaviour, and Thermal Decomposition. *Dalton Trans.* **2017**, *46*, 5644–5649. [[CrossRef](#)] [[PubMed](#)]
27. Wei, Z.; Han, H.; Filatov, A.S.; Dikarev, E.V. Changing the Bridging Connectivity Pattern within a Heterometallic Assembly: Design of Single-Source Precursors with Discrete Molecular Structures. *Chem. Sci.* **2014**, *5*, 813–818. [[CrossRef](#)]
28. Ruettinger, W.F.; Campana, C.; Dismukes, G.C. Synthesis and Characterization of Mn₄O₄L₆ Complexes with Cubane-like Core Structure: A New Class of Models of the Active Site of the Photosynthetic Water Oxidase. *J. Am. Chem. Soc.* **1997**, *119*, 6670–6671. [[CrossRef](#)]
29. Nguyen, A.I.; Ziegler, M.S.; Oña-Burgos, P.; Sturzbecher-Hohne, M.; Kim, W.; Bellone, D.E.; Tilley, T.D. Mechanistic Investigations of Water Oxidation by a Molecular Cobalt Oxide Analogue: Evidence for a Highly Oxidized Intermediate and Exclusive Terminal Oxo Participation. *J. Am. Chem. Soc.* **2015**, *137*, 12865–12872. [[CrossRef](#)] [[PubMed](#)]
30. Tsaroucha, M.; Aksu, Y.; Irran, E.; Driess, M. Synthesis of Stannyl-Substituted Zn₄O₄ Cubanes as Single-Source Precursors for Amorphous Tin-Doped ZnO and Zn₂SnO₄ Nanocrystals and Their Potential for Thin Film Field Effect Transistor Applications. *Chem. Mater.* **2011**, *23*, 2428–2438. [[CrossRef](#)]
31. Piga, F.; Moro, F.; Krivokapic, I.; Blake, A.J.; Edge, R.; McInnes, E.J.L.; Evans, D.J.; McMaster, J.; Van Slageren, J. Magnetic Properties of a Novel Family of Ferrous Cubanes. *Chem. Commun.* **2012**, *48*, 2430–2432. [[CrossRef](#)] [[PubMed](#)]
32. Navulla, A.; Huynh, L.; Wei, Z.; Filatov, A.S.; Dikarev, E.V. Volatile Single-Source Molecular Precursor for the Lithium Ion Battery Cathode. *J. Am. Chem. Soc.* **2012**, *134*, 5762–5765. [[CrossRef](#)]
33. Magnus, P.; Payne, A.H.; Waring, M.J.; Scott, D.A.; Lynch, V. Conversion of α , β -Unsaturated Ketones into α -Hydroxy Ketones Using an Mn^{III} Catalyst, Phenylsilane and Dioxygen: Acceleration of Conjugate Hydride Reduction by Dioxygen. *Tetrahedron Lett.* **2000**, *41*, 9725–9730. [[CrossRef](#)]
34. Perdew, J.P.; Burke, K.; Ernzerhof, M. Generalized gradient approximation made simple. *Phys. Rev. Lett.* **1996**, *77*, 3865. [[CrossRef](#)] [[PubMed](#)]

35. Weigend, F.; Ahlrichs, R. Balanced Basis Sets of Split Valence, Triple Zeta Valence and Quadruple Zeta Valence Quality for H to Rn: Design and Assessment of Accuracy. *Phys. Chem. Chem. Phys.* **2005**, *7*, 3297–3305. [[CrossRef](#)]
36. Neese, F.; Wennmohs, F.; Becker, U.; Riplinger, C. The ORCA Quantum Chemistry Program Package. *J. Chem. Phys.* **2020**, *152*. [[CrossRef](#)] [[PubMed](#)]
37. Lu, T.; Chen, F. Multiwfn: A Multifunctional Wavefunction Analyzer. *J. Comput. Chem.* **2012**, *33*, 580–592. [[CrossRef](#)] [[PubMed](#)]

Disclaimer/Publisher’s Note: The statements, opinions and data contained in all publications are solely those of the individual author(s) and contributor(s) and not of MDPI and/or the editor(s). MDPI and/or the editor(s) disclaim responsibility for any injury to people or property resulting from any ideas, methods, instructions or products referred to in the content.